JACS JOURNAL OF THE AMERICAN CHEMICAL SOCIETY

Article

Cite This: J. Am. Chem. Soc. 2018, 140, 17580−17590

pubs.acs.org/JACS

Enzyme Architecture: Breaking Down the Catalytic Cage that Activates Orotidine 5′-Monophosphate Decarboxylase for Catalysis

Archie C. Reyes,[†] David C. Plache,[†] Astrid P. Koudelka,[†] Tina L. Amyes,[†] John A. Gerlt,[‡] and John P. Richard*[,†]

[†]Department of Chemistry, University at Buffalo, SUNY, Buffalo, New York 14260-3000, United States

[‡]Department of Chemistry and Biochemistry, University of Illinois, Urbana, Illinois 61801, United States

Supporting Information

ABSTRACT: We report the results of a study of the catalytic role of a network of four interacting amino acid side chains at yeast orotidine 5′-monophosphate decarboxylase (*Sc*OMPDC), by the stepwise replacement of all four side chains. The H-bond, which links the $-CH_2OH$ side chain of S154 from the pyrimidine umbrella loop of *Sc*OMPDC to the amide side chain of Q215 in the phosphodianion gripper loop, creates a protein cage for the substrate **OMP**. The role of this interaction in optimizing transition state stabilization from the dianion gripper side chains Q215, Y217, and R235 was probed by determining the kinetic parameter k_{cat}/K_m for 16 enzyme variants, which include all combinations of single, double, triple, and quadruple S154A, Q215A, Y217F, and R235A mutations. The effects of consecutive Q215A, Y217F, and R235A mutations on $\Delta G^{‡}$ for wild-type enzyme-catalyzed decarboxylation sum to 11.6 kcal/mol, but to only 7.6 kcal/mol when starting from S154A mutant. This shows that the S154A mutation results in a (11.6−7.6) = 4.0 kcal/mol decrease in transition state stabilization from interactions with Q215, Y217, and R235. Mutant cycles show that ca. 2 kcal/mol of this 4 kcal/mol effect is from the direct interaction between the S154 and Q215 side chains and that ca. 2 kcal/mol is from a tightening in the stabilizing interactions of the Y217 and R235 side chains. The sum of the effects of individual A154S, A215Q, F217Y and A235R substitutions at the quadruple mutant of *Sc*OMPDC to give the corresponding triple mutants, 5.6 kcal/mol, is much smaller than 16.0 kcal/mol, the sum of the effects of the related four substitutions in wild-type *Sc*OMPDC to give the respective single mutants. The small effect of substitutions at the quadruple mutant is consistent with a large entropic cost to holding the flexible loops of *Sc*OMPDC in the active closed conformation.

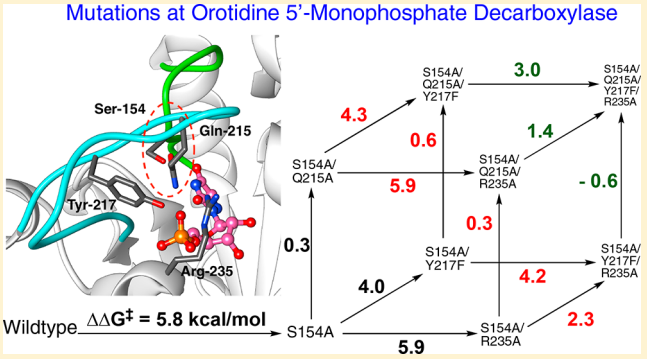

INTRODUCTION

Orotidine 5′-monophosphate decarboxylase (**OMPDC**) employs no metal ions or other cofactors, yet results in an enormous 31 kcal/mol stabilization of the transition state for the chemically very difficult decarboxylation of orotidine 5′-monophosphate (**OMP**) to give uridine 5′-monophosphate (**UMP**).[1−3] This 31 kcal/mol transition state stabilization is the sum of 12, 10, and 9 kcal/mol stabilizing interactions (Scheme 1) from the phosphodianion, ribosyl ring, and pyrimidine ring fragments of the substrate, respectively.[4] The enzymatic reaction proceeds by a stepwise mechanism, through a UMP carbanion reaction intermediate (Scheme 1), that is stabilized by ≥16 kcal/mol, relative to UMP, by interactions with the protein catalyst.[5,6]

The X-ray crystal structure for the complex between yeast **OMPDC** (*Sc*OMPDC) and the tight-binding intermediate analog 6-azauridine 5′-monophosphate (**6-azaUMP**) shows a network of interactions between the protein and ligand.[7,8] We are interested in understanding the mechanism by which interactions of the three-substrate fragments are funneled toward stabilization of the transition state for *Sc*OMPDC-catalyzed decarboxylation of the pyrimidine ring of **OMP**.[1,9]

A crucial network of amino acid side chains (Figure 1A,B) extend from the phosphodianion gripper loop shown in blue (P202 to V220) to the pyrimidine umbrella shown in green (A151 to T165) and consists of Q215, Y217, R235, and S154. These side-chains are poorly placed to interact with a hypothetical enzyme-bound transition state at the open enzyme (Figure 1A). Ligand binding drives a large enzyme conformational change to give the closed enzyme (Figure 1B), in which the side chains provide strong transition state stabilization.[10−15] This network plays at least two roles in catalysis of the decarboxylation of **OMP**. (1) The side chains of Q215, Y217, and R235 are distant from the pyrimidine ring and do not interact directly with the site of *Sc*OMPDC-catalyzed decarboxylation,[13] but promote decarboxylation by stabilizing the catalytically active closed form of *Sc*OMPDC

Received: September 5, 2018
Published: November 26, 2018

DOI: 10.1021/jacs.8b09609
J. Am. Chem. Soc. 2018, 140, 17580−17590

Scheme 1. Contribution of Individual Substrate Fragments to the Total Stabilization of the Transition State for OMPDC-Catalyzed Decarboxylation of OMP through the UMP Carbanion Reaction Intermediate

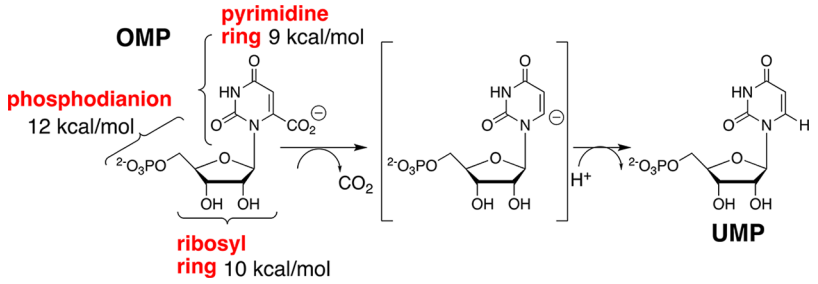

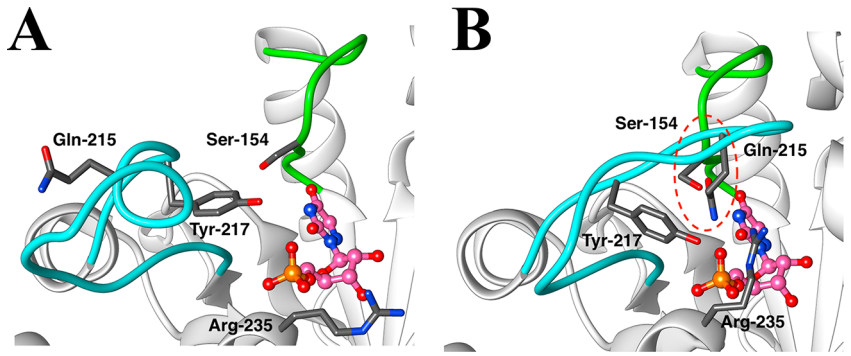

Figure 1. Comparison of the X-ray crystal structures for (A) unliganded *Sc*OMPDC (Protein Databank (PDB) entry 3GDL) and (B) the complex between *Sc*OMPDC and the tight-binding substrate analog 6-azauridine 5′-monophosphate (**6-azaUMP**) (PDB entry 3GDK). The hypothetical **6-azaUMP** ligand has been inserted in panel A to mimic the position of the ligand at panel B. (B) shows the ligand-driven movement of the phosphodianion gripper loop (P202 to 220, shaded blue) toward the pyrimidine umbrella loop (A151 to T165, shaded green) and of R235 toward the phosphodianion. The $-CH_2OH$ side chain of S154 bridges these loops and holds Q215 near the dianion by donating an H-bond to the amide side chain of Q215 and accepting an H-bond from the C-5 pyrimidine −NH (dashed red circle).

($\mathbf{E_C}$, Scheme 2) relative to the inactive open form $\mathbf{E_O}$.[9,16−18] (2) The $-CH_2OH$ side chain of S154 bridges the phosphodianion and the pyrimidine binding sites at $\mathbf{E_C}$ by donating an H-bond to the amide side chain of Q215 and accepting an H-bond from the C-5 pyrimidine −NH. These bridging interactions lock the substrate in a protein cage, by stabilizing the active closed form of *Sc*OMPDC ($\mathbf{E_C}$) relative to $\mathbf{E_O}$ (Figure 1), while holding the side chains from Q215, Y217, and R235 close to the dianion.

Scheme 2. Two-Step Mechanism for Substrate Binding to OMPDC

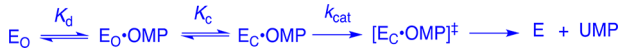

We have shown that the S154A mutation of *Sc*OMPDC results in a large 5.8 kcal/mol destabilization of the transition state for decarboxylation of **OMP** and provided evidence that S154 plays an important role in orienting Q215 to interact with the substrate phosphodianion.[15] We now address the more complex question of whether there is cooperativity between S154 and the dianion gripper side chains Y217 and R235 in stabilizing the decarboxylation transition state. We have probed the functioning of these four interacting side chains by site-directed mutagenesis. Such analyses are straightforward for small networks of two amino acid side chains,[19] but studies on networks larger that two side chains are relatively rare. These include an analysis of the role of the three lysine side chains at the KMSKS mobile loop, in catalysis by tyrosyl amino acid synthase,[20] and our recent examination of the network of three side chains (Q215, Y217, and R235) that interact with the phosphodianion of substrates bound to **OMPDC**.[11]

We are not aware of systematic mutagenesis studies on networks larger than three amino acids. This study on the S154, Q215, Y217, and R235 network (Figure 1) reports data to extend the following earlier work: (a) Studies on the effect of all single, double, and triple Q215A, Y217F, and R235A mutations on the kinetic parameters for **OMPDC** catalyzed reactions of whole substrates **OMP**,[11,21] and 5-fluoroorotidine 5′-monophosphate (**FOMP**).[10] (b) A restricted study on S154A, Q215A and S154A/Q215A mutants of **OMPDC**.[15] We report here kinetic parameters for the six additional mutant enzymes required to obtain a complete set of kinetic data for all single, double, triple, and quadruple Q215A, Y217F, R235A, and S154A mutations of *Sc*OMPDC. Our analyses of the kinetic parameter k_{cat}/K_m for decarboxylation of **OMP** and **FOMP** catalyzed by these 16 variants of *Sc*OMPDC (Scheme 3) extends protocol developed in earlier work.[10,11,15] Several lines of analysis are explored in describing the role played by the $-CH_2OH$ side chain of S154 in the efficient functioning of phosphodianion gripper side chains at the transition state for **OMPDC**-catalyzed decarboxylation.

EXPERIMENTAL SECTION

Materials. **OMP**[12,22] and **FOMP**[12,23] were prepared enzymatically by literature procedures. 3-(*N*-Morpholino)propanesulfonic acid (MOPS) and imidazole were purchased from Sigma (St. Louis, MO). Sodium hydroxide (1.0 N), hydrochloric acid (1.0 N), sodium chloride, tris(hydroxymethyl)-aminomethane (basic form), and Amicon centrifugal filter units with a 10K molecular weight cutoff

DOI: 10.1021/jacs.8b09609
J. Am. Chem. Soc. 2018, 140, 17580−17590

Scheme 3. Wild-Type *Sc*OMPDC and All Possible Single, Double, Triple and Quadruple Q215A, Y217F, R235A, and S154A Mutants Enzymes[a]

Wild Type *Sc*OMPDC

Singles	Doubles	Triples
	Q215A/Y217F	
Q215A	Q215A/R235A	Q215A/Y217F/R235A
Y217F	Q215A/S154A	S154A/Q215A/Y217F*
R235A	Y217F/R235A	S154A/Q215A/R235A*
S154A	S154A/Y217F*	S154A/Y217F/R235A*
	S154A/R235A*	

Quadruple: S154A/Q215A/Y217F/R235A*

[a]Asterisks show the new mutant enzymes prepared for this work.

(MWCO) were purchased from Fisher (Hampton, NH). Nickel chloride hexahydrate was a generous gift from Prof. Andrew Murkin (University at Buffalo, Buffalo, NY). Chelating Sepharose Fast-Flow and Q-Sepharose were purchased from GE Healthcare (Marlborough, MA). Water was purified using a Milli-Q Academic purification system from EMD Millipore (Burlington, MA). All other commercial chemicals were reagent-grade or better and were used without further purification.

Preparation of Wild-Type and Mutant Yeast Orotidine 5′-Monophosphate Decarboxylases. The plasmid p*Sc*ODC-15b containing the gene encoding wild-type orotidine 5′-monophosphate decarboxylase from *Saccharomyces cerevisiae* (*Sc*OMPDC) with an N-terminal His_6-tag was available from earlier studies.[15,24] The protein sequence differs from the published sequence for wild-type *Sc*OMPDC by the following mutations: S2H, C155S, A160S, and N267D.[15,24] The kinetic parameters for this preparation of wild-type *Sc*OMPDC are in agreement with those reported by Porter and Short.[25] The C155S mutation has been shown to result in a more stable protein.[26]

Site-directed mutagenesis on p*Sc*ODC-15b was carried out using the QuikChange II kit from Stratagene (San Diego, CA). The procedures for the preparation of the S154A,[15] Q215A,[15] R235A,[14] Y217F,[13] S154A/Q215A,[15] Q215A/Y217F,[13] Q215/R235A,[13] Y217F/R235A,[13] and Q215A/Y217F/R235A[13] mutants were described in earlier work. The following primers, with the altered codons underlined, were used to prepare the new mutant enzymes from previously prepared mutants of *Sc*OMPDC.

5′-GACGCATTGGGTCAACAG**TTT**AGAACCGTGGATG-ATGTGG-3′ was used to introduce the Y217F mutation into the plasmid for the S154A mutant enzyme to yield the plasmid for the S154A/Y217F mutant.

5′-GGATCTGACATTATTATTGTTGGA**GCA**GGACT-ATTTGCAAAGGG-3′ was used to introduce the R235A mutation into the plasmid for the S154A/Q215A mutant enzyme to yield the plasmid for the S154A/Q215A/R235A mutant.

5′-GGCCTTTTGATGTTAGCAGAATTG**GCA**TCTAAG-GGCTCCC-3′ was used to introduce the S154A mutation into the plasmids for the R235A, Q215A/Y217F, Y217F/R235A, and Q215A/Y217F/R235A mutant enzymes to yield the plasmids for the S154A/R235A, S154A/Q215A/Y217F, S154A/Y217F/R235A, and S154A/Q215A/Y217F/R235A mutant enzymes, respectively.

The mutants of *Sc*OMPDC were overexpressed, after transformation of *E. coli* BL21 (DE3) with the appropriate plasmid. The proteins were purified as described previously,[11,15] except that passage over the Chelating Sepharose Fast-Flow column was repeated a second time to ensure complete removal of host *E. coli* **OMPDC**. The fractions from the second Sepharose Fast-Flow column were treated with thrombin to remove the N-terminal His_6-tag, and this tag was separated from the protein by purification over a column of Q-sepharose. Wild-type **OMPDC** from *E. coli* (*Ec*OMPDC) was prepared and purified according to published procedures.[27]

Preparation of Solutions. The solution pH was determined at 25 °C using an Orion Model 720A pH meter equipped with a Radiometer pHC4006−9 combination electrode that was standardized at pH 4.00, 7.00, and 10.00 at 25 °C. Stock solutions of **OMP** (20 mM) and **FOMP** (20 mM) were prepared by dissolving the solid nucleotide in water and adding 1 N HCl or 1 N NaOH to adjust the solution to the desired pH. These solutions were stored at −20 °C. The concentration of **OMP** in 0.1 M HCl was determined from the absorbance at 267 nm using a value of ε = 9430 M^{-1} cm^{-1}.[28] The concentration of **FOMP** in 0.1 M HCl was determined from the absorbance at 271 nm using a value of ε = 10 200 M^{-1} cm^{-1}.[5]

Solutions of MOPS buffers (50% free base) were prepared by addition of measured amounts of 1 N NaOH and solid NaCl to give the desired ratio of acidic and basic buffer forms, and solution ionic strength. Stock solutions (20−40 mg/mL) of mutant *Sc*OMPDC were dialyzed exhaustively against 10 mM MOPS at pH 7.0 (50% free base), 4 °C and I = 0.105 (NaCl). The solutions were further concentrated using Amicon filter units, when necessary. The concentration of *Sc*OMPDC in these solutions was determined from the absorbance at 280 nm for wild type OMPDC, and values of ε = 29 900 or 28 400 M^{-1} cm^{-1} for Y217F mutant enzymes, that were calculated using the ProtParam tool available on the ExPASy server.[29,30]

Kinetic Parameters for Decarboxylation of OMP. The decarboxylation of **OMP** was monitored spectrophotometrically by following the decrease in absorbance at 279, 290, 295, or 300 nm [$\Delta\varepsilon$, λ: − 2400 M^{-1} cm^{-1}, 279 nm; − 1620 M^{-1} cm^{-1}, 290 nm; − 840 M^{-1} cm^{-1}, 295 nm; − 344 M^{-1} cm^{-1}, 300 nm]. The wavelength was chosen to give an initial absorbance of ≤2.0. These reactions were monitored at the following wavelengths: [**OMP**] ≤ 0.08 mM, 279 nm; [**OMP**] = 0.1−0.3 mM, 290 nm; [**OMP**] = 0.3−0.8 mM, 295 nm; [**OMP**] ≥ 1 mM, 300 nm. Assays for mutant *Sc*OMPDC-catalyzed decarboxylation of **OMP** were at 25 °C, pH 7.1 (10 mM MOPS) and I = 0.105 (NaCl). Reactions (1.0 mL) were initiated by addition of 10−60 μL of a stock solution of mutant *Sc*OMPDC to give the following concentrations of mutant enzyme: 0.025 mM, S154A/Y217F mutant; 0.2 mM, S154A/R235A mutant; 0.1 mM, S154A/Q215A/Y217F mutant; and 0.2 mM, S154A/Q215A/R235A mutant. The initial velocity v (M s^{-1}) for mutant *Sc*OMPDC-catalyzed decarboxylation of **OMP** (0.03−3.0 mM) was determined by monitoring the decrease in absorbance at the chosen wavelength for the decarboxylation of 5−10% of total **OMP**. Values of k_{cat}/K_m (M^{-1} s^{-1}) were obtained from the nonlinear least-squares fits of four or more values of v/[E] (s^{-1}) to the appropriate kinetic equation.

Kinetic Parameters for Decarboxylation of FOMP. Assays for wild-type *Ec*OMPDC-catalyzed decarboxylation of **FOMP** were conducted at 25 °C and pH 7.1 (10 mM MOPS) and at I = 0.105 (NaCl). Reactions (1.0 mL) were initiated by the addition of 2−4 μL of a stock solution of wild-type *Ec*OMPDC to give a final enzyme concentration of 5−10 nM. The initial velocity v (M s^{-1}) for wild-type *Ec*OMPDC-catalyzed decarboxylation of **FOMP** (10−200 μM) was determined by monitoring the decrease in absorbance at 282 nm [$\Delta\varepsilon$ = −2400 M^{-1} cm^{-1}] for the decarboxylation of 5−10% total **FOMP**. The value of the kinetic parameter k_{cat}/K_m (M^{-1} s^{-1}) was obtained as the slope of the linear plot of values of v/[E] (s^{-1}) against [FOMP].

Mutant *Sc*OMPDC-catalyzed decarboxylation of **FOMP** was monitored spectrophotometrically over 5−10 half-reaction times and working at a wavelength (282 or 300 nm) where the total initial absorbance for **FOMP** and mutant *Sc*OMPDC is ≤2.0. Time courses for mutant *Sc*OMPDC-catalyzed decarboxylation of **FOMP** were obtained at 25 °C and pH 7.1 (10 mM MOPS) and at I = 0.105 (NaCl). Reactions (1.0 mL) containing 60−150 μM **FOMP** were initiated by addition of 3−40 μL of a stock solution of the mutant *Sc*OMPDC to give the following enzyme concentrations: 3 μM, S154A/Y217F mutant; 20 μM, S154A/R235A mutant; 10 μM, S154A/Q215A/Y217F mutant; 5−10 μM, S154A/Q215A/R235A mutant; 0.2 mM, S154A/Y217F/R235A mutant; and 0.1 mM, S154A/Q215A/Y217F/R235A mutant. The rate constants k_{obs} (s^{-1}) for the pseudo-first-order decay of **FOMP** to FUMP were obtained by fitting the plot of absorbance A against time to the equation for an exponential decay. Values of the second-order rate constant k_{cat}/K_m

DOI: 10.1021/jacs.8b09609
J. Am. Chem. Soc. 2018, 140, 17580−17590

(M^{-1} s^{-1}) for *Sc*OMPDC-catalyzed decarboxylation of **FOMP** were then calculated from the relationship $k_{cat}/K_m = k_{obs}/[E]$.

RESULTS

Figure S1 shows the linear plot of $v/[E]$ against [**FOMP**] for *Ec*OMPDC-catalyzed decarboxylation of **FOMP**, with the slope of $k_{cat}/K_m = 2.7 \times 10^6$ M^{-1} s^{-1}. The observation of a linear plot through [**FOMP**] = 0.2 mM shows that $K_m \gg 0.2$ mM. By comparison, values of $k_{cat} = 14$ s^{-1} and $k_{cat}/K_m = 6.4 \times 10^5$ M^{-1} s^{-1} were reported for *Ec*OMPDC-catalyzed decarboxylation of **OMP**.[27] We conclude that the C-5 fluorine of **FOMP** results in a 4-fold increase in k_{cat}/K_m for *Ec*OMPDC-catalyzed decarboxylation.

Figure 2A shows plots of $v/[E]$ against [**OMP**] for decarboxylation catalyzed by the S154A/Q215A/Y217F

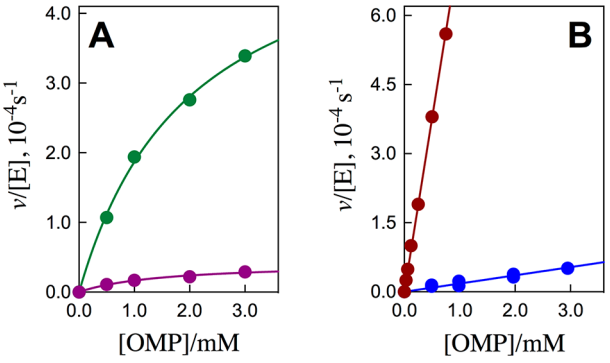

Figure 2. Dependence of $v/[E]$ (s^{-1}) for decarboxylation of **OMP** catalyzed by mutant forms of *Sc*OMPDC on the concentration of **OMP** for reactions at 25 °C, pH 7.1 (10 mM MOPS) and at $I = 0.105$ (NaCl). (A) Green symbols, S154A/Q215A/Y217F mutant; purple symbols, S154A/R235A mutant. (B) Maroon symbols, S154A/Y217F mutant; blue symbols, S154A/Q215A/R235A mutant.

(green symbols) and S154A/R235A (purple symbols) mutants of *Sc*OMPDC, and Figure 2B show similar plots for the S154A/Y217F (maroon symbols) and S154A/Q215A/R235A (blue symbols) mutants. The solid lines in Figure 2 show the fits of these experimental data to the full Michaelis–Menten equation (Figure 2A) or the linear form of this equation, where $K_m \gg$ [**OMP**] (Figure 2B). The kinetic parameters from Figure 2A require that <10% of total **OMP** is tied up as the Michaelis complex (Table S1). The concentration of free **OMP** is therefore essentially equal to total [**OMP**] (Figure 2A).

Figure 3 shows time courses for the change in absorbance at 300 nm for decarboxylation of **FOMP** catalyzed by S154A/Y217F/R235A (Figure 3A) and S154A/Q215A/Y217F/R235A mutants of *Sc*OMPDC (Figure 3B). Figure S2A–D shows time-courses for the change in absorbance at 282 nm for decarboxylation of **FOMP** catalyzed by the S154A/Y217F (Figure S2A), S154A/R235A (Figure S2B), S154A/Q215/Y217F (Figure S2C), and the S154A/Q215A/R235A (Figure S2D) mutants of *Sc*OMPDC. The fits of the experimental data for each Figure to the exponential decay for the pseudo-first-order enzyme-catalyzed reaction of **FOMP** gives the observed first order rate constant k_{obs} (s^{-1}) for *Sc*OMPDC-catalyzed decarboxylation. The fits to a simple exponential decay show that these mutant *Sc*OMPDC-catalyzed decarboxylation reactions are first order in [**FOMP**] (0.06–0.15 mM $\ll K_m$). Each of the experiments from Figures 3 and S2 were repeated

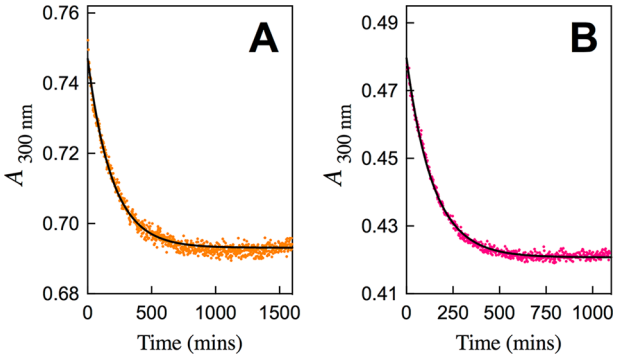

Figure 3. Full time-course for the decarboxylation of **FOMP** catalyzed by mutants of *Sc*OMPDC for reactions at 25 °C, pH 7.1 (10 mM MOPS) and at $I = 0.105$ (NaCl). (A) Decarboxylation of 0.10 mM **FOMP** catalyzed by 0.20 mM of the S154A/Y217F/R235A mutant of *Sc*OMPDC. (B) Decarboxylation of 0.10 mM **FOMP** catalyzed by 0.10 mM of the S154A/Q215A/Y217F/R235A mutant of *Sc*OMPDC.

two or more times, and the values of $k_{obs}/[E]$ for each mutant *Sc*OMPDC-catalyzed decarboxylation were found to be reproducible to better than ±10%.

The new values of k_{cat}/K_m for decarboxylation of **OMP** catalyzed by mutant forms of *Sc*OMPDC, which were obtained from the fits of data shown in Figure 2 to the appropriate kinetic equation, are shown in bold type in Table 1. The fits from Figure 2A also gave values of $K_m = 2.0 \pm 0.2$ mM for the S154A/R235A mutant and 1.5 ± 0.05 mM for the S154A/Q215A/Y217F mutant. Table 1 reports values of k_{cat}/K_m determined in earlier work for decarboxylation of **OMP** catalyzed by wild-type *Sc*OMPDC and mutants of *Sc*OMPDC.[11,15] The new values of k_{cat}/K_m for decarboxylation of **FOMP** catalyzed by mutant forms of *Sc*OMPDC, obtained from the fits of data shown in Figures 3 and S1, are shown in bold type Table 1. Table 1 reports values of k_{cat}/K_m determined in earlier work for decarboxylation of **FOMP** catalyzed by wild-type *Sc*OMPDC and mutants of *Sc*OMPDC, to give data for all possible single, double, triple, and quadruple S154A, Q215A, Y217F, and R235A mutations.[10] Table 1 also reports rate constant ratios $\frac{(k_{cat}/K_m)_F}{(k_{cat}/K_m)_H}$ for wild-type and mutant *Sc*OMPDC-catalyzed decarboxylation of **FOMP** and **OMP**.

There was no detectable decarboxylation of 1.0 mM **OMP** ($[\Delta A_{300} \leq 0.03$) catalyzed by 0.2 mM of the S154A/Y217F/R235A or S154A/Q215A/Y217F/R235A mutants over a 20 h reaction time. This shows that $k_{cat}/K_m < 0.006$ M^{-1} s^{-1} for the mutant enzyme-catalyzed decarboxylation reactions. Large limiting ratios $\frac{(k_{cat}/K_m)_F}{(k_{cat}/K_m)_H}$ are observed for reactions catalyzed by severely impaired mutants of *Sc*OMPDC, where the relative reaction barriers are determined by chemical reactivity of enzyme-bound **OMP** and **FOMP**.[10] The ratio of $\frac{(k_{cat}/K_m)_F}{(k_{cat}/K_m)_H} = 700 \pm 200$ is the average of the ratios from Table 1 for severely impaired mutants where $(k_{cat}/K_m)_H \leq 1.0$ M^{-1} s^{-1} (S154A/Y217F, S154A/R235A, S154A/Q215A/Y217F, S154A/Q215A/R235A, and Q215A/Y217F/R235A). The values of $(k_{cat}/K_m)_H$ for decarboxylation catalyzed by the S154A/Y217F/R235A and S154A/Q215A/Y217F/R235A mutants, shown in underlined type in Table 1, were estimated from the value $(k_{cat}/K_m)_F$ for decarboxylation of **FOMP** and the rate constant ratio $\frac{(k_{cat}/K_m)_F}{(k_{cat}/K_m)_H} = 700 \pm 200$.

DOI: 10.1021/jacs.8b09609
J. Am. Chem. Soc. 2018, 140, 17580–17590

Table 1. Kinetic Parameters for *Sc*OMPDC-Catalyzed Decarboxylation of OMP and FOMP[a]

	OMP[b]		FOMP[c]		
*Sc*OMPDC	k_{cat}/K_m (M^{-1} s^{-1})	$\Delta\Delta G^{\ddagger}$ (kcal/mol)[d]	k_{cat}/K_m (M^{-1} s^{-1})	$\Delta\Delta G^{\ddagger}$ (kcal/mol)[d]	$\frac{(k_{cat}/K_m)_F}{(k_{cat}/K_m)_H}$[e]
wild-type	1.1×10^7		1.2×10^7		1.1
Q215A	2.6×10^5	2.2	2.0×10^6	1.1	7.7
Y217F	1.8×10^5	2.4	1.1×10^6	1.4	6.1
R235A	910	5.6	1.6×10^5	2.6	180
S154A	630	5.8	2.9×10^5	2.2	460
S154A/Q215A	380	6.1	7.7×10^4	3.0	200
S154A/Y217F	**0.75 ± 0.01**	9.8	**520 ± 10**	5.9	700
S154A/R235A	**0.027 ± 0.004**	11.7	**20 ± 2**	7.9	740
Q215A/Y217F	3.4×10^3	4.8	5.3×10^4	3.2	16
Q215A/R235A	14	8.0	7200	4.4	510
Y217F/R235A	4.1	8.8	820	5.7	200
S154A/Q215A/Y217F	**0.28 ± 0.02**	10.4	**250 ± 10**	6.4	890
S154A/Q215A/R235A	**0.018 ± 0.001**	12.0	**10 ± 1**	8.3	560
S154A/Y217F/R235A	0.0006 ± 0.0002[f]	14.0	**0.44 ± 0.02**	10.1	
Q215A/Y217F/R235A	0.037	11.6	28	7.7	760
S154A/Q215A/Y217F/R235A	0.0016 ± 0.0005[f]	13.4	**1.1 ± 0.1**	9.6	

[a]Conditions: pH 7.1 (10 mM MOPS), 25 °C and I = 0.105 (NaCl). [b]The new values for this manuscript are in bold type. The other rate constants are from ref 11 or 15. The quoted uncertainty is the standard error from the least-squares fit of the kinetic data to the appropriate kinetic equation. [c]The new values for this manuscript are in bold type. The other rate constants are from ref 10.The quoted uncertainty in the original values is the average of two or more determinations of k_{cat}/K_m. [d]Calculated from the ratio of the values of k_{cat}/K_m for wild-type and mutant *Sc*OMPDC-catalyzed decarboxylation of **OMP** or **FOMP**. [e]The ratio of the values of k_{cat}/K_m for **OMPDC**-catalyzed decarboxylation of **OMP** and **FOMP**. [f]No detectable activity toward decarboxylation of **OMP**: $k_{cat}/K_m < 0.006$ M^{-1} s^{-1}. The rate constants were estimated from k_{cat}/K_m for mutant enzyme-catalyzed decarboxylation of **FOMP** (see text). The range of values is calculated from the estimated uncertainty of ±50% in $\frac{(k_{cat}/K_m)_F}{(k_{cat}/K_m)_H}$ for **OMPDC**-catalyzed decarboxylation of **OMP** and **FOMP**.

DISCUSSION

All of the newly reported mutants of *Sc*OMPDC were expressed in *E.* Coli that contained host *Ec*OMPDC. These mutants were prepared with an N-terminal His_6-tag, and with two passes over a chelating column to ensure complete removal of *Ec*OMPDC host enzyme. The value of $\frac{(k_{cat}/K_m)_F}{(k_{cat}/K_m)_H} > 67$ (Table 1) for the most severely impaired S154A/Y217F/R235A mutant, which shows no activity toward decarboxylation of **OMP**, is much larger than the value for *Ec*OMPDC, $\frac{(k_{cat}/K_m)_F}{(k_{cat}/K_m)_H} = 4$. This shows that there is no significant (<10%) decarboxylation of **FOMP** by wild-type *Ec*OMPDC from the host organism. If, for example, 10% of the observed activity of this preparation toward decarboxylation of **FOMP** were due to wild-type host **OMPDC**, then a detectable value of $\frac{(k_{cat}/K_m)_F}{(k_{cat}/K_m)_H} = (1.00)/[0.10][0.25] = 40$ would have been observed.

The <2-fold variation in the 5-F substituent effect on decarboxylation reactions catalyzed by severely impaired mutants of *Sc*OMPDC [$(k_{cat}/K_m)_{OMP} \leq 1.0$ M^{-1} s^{-1}, $\frac{(k_{cat}/K_m)_F}{(k_{cat}/K_m)_H} = 560-890$) shows that the value of $(k_{cat}/K_m)_F$ for these mutant enzymes establishes $(k_{cat}/K_m)_H$ to within a factor of 2. The rate constants $(k_{cat}/K_m)_H$ for decarboxylation reactions catalyzed by the S154A/Y217F/R235A and S154A/Q215A/Y217F/R235A mutants, that were too slow to be detected [$(k_{cat}/K_m)_H < 0.006$ M^{-1} s^{-1}], were estimated from the value of $(k_{cat}/K_m)_F$ (Table 1) and $\frac{(k_{cat}/K_m)_F}{(k_{cat}/K_m)_H} = 700$.

This study of the effect of mutations of S154, Q215, Y217, and R235 will provide a clear description of the role of this network in catalysis, provided the effects are restricted to the elimination of interactions between the transition state and the excised side chain(s). The following observations provide strong evidence that there only minimal effects of these mutations on $[(k_{cat}/K_m)_H$ that arise from protein structural changes that perturb protein-transition state interactions. (1) Single Q215A, Y217F, and R235A mutations result in negligible (≤0.5 kcal/mol) changes in the activation barrier to **OMPDC**-catalyzed decarboxylation of the phosphodianion truncated substrate 1-(β-erythrofuranosyl)orotic acid (**EO**, Scheme 4).[13] This provides strong evidence that the single

Scheme 4. Stepwise OMPDC-Catalyzed Decarboxylation of Phosphodianion Truncated Substrate EO

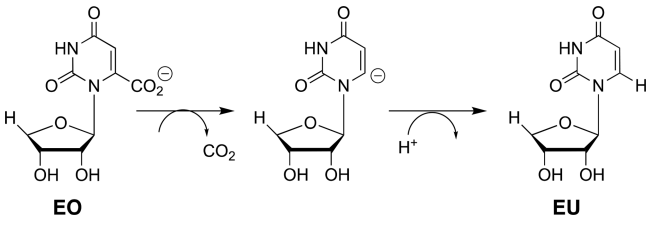

mutations have no effect on the structural integrity and catalytic activity at the site of decarboxylation of the pyrimidine ring, and are restricted to the loss of protein dianion interactions at the dianion activation site. (2) The sum of the effects of the four single S154A, Q215A, Y217F, and R235A mutations on the activation barrier $\Delta G^{\ddagger}$ for decarboxylation catalyzed by wild-type **OMPDC** is 16.0 kcal/mol (Table 1). By comparison, there is only a 13.4 kcal/mol difference between the activation barriers $\Delta G^{\ddagger}$ for wild type and the S154A/Q215A/Y217F/R235A quadruple

DOI: 10.1021/jacs.8b09609
J. Am. Chem. Soc. 2018, 140, 17580−17590

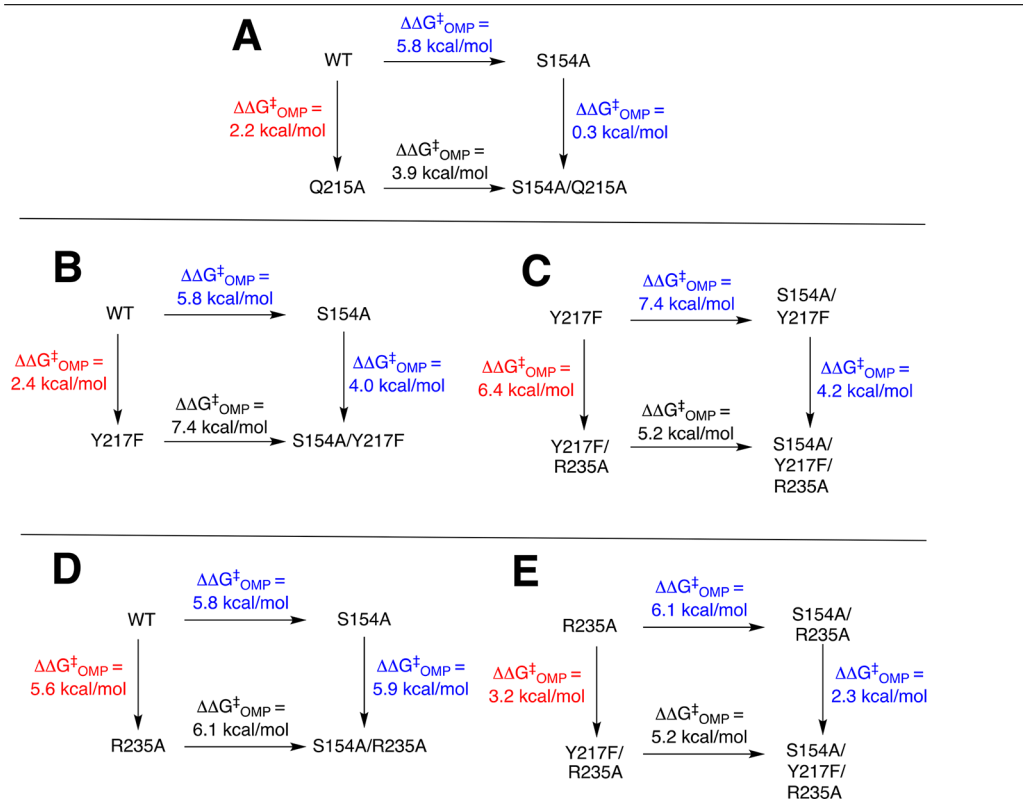

Figure 4. Mutant cycles that show the effect of S154A mutations on: (A) stabilization of the transition state for wild-type *Sc*OMPDC-catalyzed decarboxylation of **OMP** by interactions with Q215; (B) stabilization of the transition state for wild-type *Sc*OMPDC-catalyzed decarboxylation of **OMP** by interactions with Y217F; (C) stabilization of the transition state for Y217F *Sc*OMPDC-catalyzed decarboxylation of **OMP** by interactions with R235; (D) stabilization of the transition state for wild-type *Sc*OMPDC-catalyzed decarboxylation of **OMP** by interactions with R235A; (E) stabilization of the transition state for R235A *Sc*OMPDC-catalyzed decarboxylation of **OMP** by interactions with Y217F.

mutant enzyme-catalyzed decarboxylation of **OMP** (Table 1) This shows that there can be no large additional increase in the activation barrier of **OMPDC**-catalyzed decarboxylation associated with the simultaneous mutations of the S154A, Q215A, Y217F, and R235A, compared with the mutation of single side chains. (3) Q215A mutations result in a ca. 2 kcal/mol destabilization of the transition state for decarboxylation of **OMP** when S154 is present and in a smaller ca. 0.3 kcal/mol destabilization when S154 is absent, as discussed in detail below. The exception is the Q215A mutation of the S154A/Y217F/R235A variant, which results in a ca. 0.5 kcal/mol stabilization or the transition state for *Sc*OMPDC-catalyzed decarboxylation of **FOMP**. This is consistent with a shift in the position of the Q215 side chain at the S154A/Y217F/R235A triple mutant, which alters the interaction of the protein with the decarboxylation transition state. Aside from this minor effect, we are able to rationalize the other effects of S154A, Q215A, Y217F, and R235A mutations by a consideration of the loss in transition state stabilization from interaction with the deleted side chains.

Mutant Boxes. We begin by examining two-dimensional mutant cycles (Figure 4) constructed from data in Table 1. These cycles show the effects of mutations of S154, which links the pyrimidine umbrella and phosphodianion gripper loops (Figure 1), on the stabilizing interactions between individual phosphodianion gripper side chains Q215, Y217, and R235 and the decarboxylation transition state (Figure 5).

Q215 (Figure 4A). The Q215A mutation results in a 2.2 kcal/mol destabilization of the transition state for wild-type

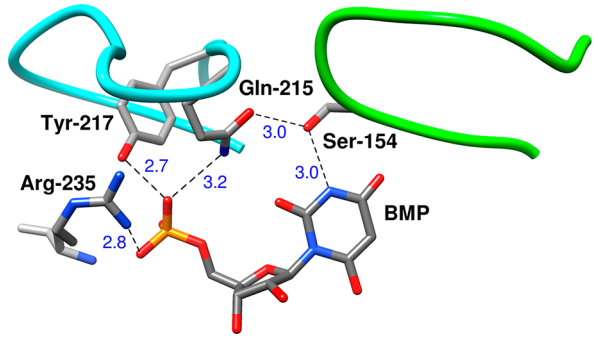

Figure 5. Representation of the X-ray crystal structure of a complex between **OMPDC** and the intermediate analog 6-hydroxyuridine 5′-monophosphate (**BMP**, PDB entry 1DQX). Phosphodianion gripper loop is shaded blue, and the pyrimidine umbrella loop is shaded green. These loops are clamped over the substrate by the following network of hydrogen bonding interactions: (a) H-bonds between the Q215, Y217, and R235 side chains and the ligand phosphodianion; (b) H-bonds that link the $-CH_2OH$ side chain of S154 to the amide side chain of Q215 and to the pyrimidine nitrogen. All distances are in Ångstroms.

*Sc*OMPDC-catalyzed decarboxylation of **OMP**, but the same mutation of the S154A mutant enzyme results in a much smaller 0.3 kcal/mol transition state destabilization.[15] This provides strong evidence that a hydrogen bond between the $-CH_2OH$ group of S154 and the amide side-chain of Q215 (Figure 1) positions the Q215 side to interact with the phosphodianion of **OMP**.

DOI: 10.1021/jacs.8b09609
J. Am. Chem. Soc. 2018, 140, 17580−17590

Table 2. Effect of Single Substitutions of Amino Acid Residues X on the Activation Barrier $(\Delta G^{\ddagger})_{OMP}$ for Decarboxylation of OMP Catalyzed by Wild-Type *Sc*OMPDC and by Previously Mutated *Sc*OMPDC[a]

	$(\Delta\Delta G^{\ddagger}_{X})_{OMP}$ (kcal/mol)[b]				
enzyme	X = Q215A	X = Y217F	X = R235A	X = S154A	$\Sigma(\Delta\Delta G^{\ddagger}_{X})_{OMP}$[c]
wild type[d]	2.2	2.4	5.6	5.8	16.0
triple mutant[e]	**−0.6**	**1.4**	**3.0**	**1.8**	5.6
single mutant[f]	2.4 (Y217F)	2.6 (Q215A)	5.8 (Q215A)	3.9 (Q215A)	
	2.4 (R235A)	3.2 (R235A)	6.4 (Y217F)	7.4 (Y217F)	
	0.3 (S154A)	4.0 (S154A)	5.9 (S154A)	6.1 (R235A)	
	2.8 (Y217F/R235A)	3.6 (Q215A/R235A)	6.8 (Q215A/Y217F)	5.6 (Q215A/Y217F)	
double mutant[g]	0.6 (S154A/Y217F)	4.3 (S154A/Q215A)	5.9 (S154A/Q215A)	4.0 (Q215A/R235A)	
	0.3 (S154A/R235A)	2.3 (S154A/R235A)	4.2 (S154A/Y217F)	5.2 (Y217F/R235A)	

[a]For **OMPDC**-catalyzed decarboxylation at 25 °C, pH 7.1 (10 mM MOPS), and ionic strength of 0.105 (NaCl). The respective substitutions that cause the largest and smallest changes in $(\Delta G^{\ddagger})_{OMP}$ are shown in underlined and bold text, respectively. [b]Calculated from the ratio of values of k_{cat}/K_m for the precursor and mutant enzymes. [c]Sum of the effects of the S154A, Q215A, Y217F, and R235A substitutions on $(\Delta\Delta G^{\ddagger}_{X})_{OMP}$. [d]Effect of the first mutation X on the activation barrier for wild-type **OMPDC**-catalyzed decarboxylation of **OMP**. [e]Effect of the final mutation X on the activation barrier for the decarboxylation reaction catalyzed by the corresponding triple mutant of **OMPDC**. [f]Effect of the mutation X on the activation barrier for the decarboxylation reaction catalyzed by the **OMPDC** mutant given in parentheses. [g]Effect of the mutation X on the activation barrier for the decarboxylation reaction catalyzed by the **OMPDC** double mutant given in parentheses.

Y217 (Figure 4B,C). The Y217F mutation results in a 2.4 kcal/mol destabilization of the transition state for wild-type **OMPDC**-catalyzed decarboxylation of **OMP**, but the same mutation of S154A mutant *Sc*OMPDC results in a larger 4.0 kcal/mol destabilization (Figure 4B). We conclude that the H-bond between the CH_2OH group of S154 and the amide side-chain of Q215 at wild-type *Sc*OMPDC fixes the position of Y217 and R235 at the phosphodianion. This clamp is largely maintained at the Y217F mutant, where the effect is limited to the loss of the interactions of the single side chain. The clamp is released by the S154A mutation, so now the second Y217F mutation results in both the loss of the interactions to Y217 and in a weakening of the interactions to R235. The R235A mutation of Y217F *Sc*OMPDC results in a 6.4 kcal/mol transition state destabilization, but the same mutation of the S154A/Y217F mutant results in a smaller 4.2 kcal/mol transition state destabilization (Figure 4C). This provides direct evidence that the double S154A/Y217F mutation leads to a weakening of the transition state stabilization by the remaining R235 side chain.

Interaction of R235 (Figure 4D,E). The R235A mutation results in a 5.6 kcal/mol destabilization of the transition state for wild-type *Sc*OMPDC-catalyzed decarboxylation of **OMP**, but the same mutation of the S154A mutant enzyme results in a larger 5.9 kcal/mol transition state destabilization (Figure 4D), consistent with conclusion that the R235A mutation of S154A *Sc*OMPDC results in the loss of the interaction of the mutated R235 side chain, and a small weakening of the interaction with Y217F. The Y217F mutation of R235A *Sc*OMPDC results in a 3.2 kcal/mol kcal/mol transition state destabilization, but the same mutation of the S154A/R235A mutant results in only an estimated 2.3 kcal/mol destabilization (Figure 4E). This suggests that the double S154A/R235A mutation leads to a weakening of the transition state stabilization by the remaining Y217 side chain.

In conclusion, S154 plays both a specific and a general role in promoting interactions between **OMPDC** and dianion gripper side chains. The $-CH_2OH$ side chain plays the specific role of holding the amide side chain of Q215 in a position to interact with the substrate dianion. The side chain acts globally to optimize interactions with Y217 and R235 by locking the substrate in the protein cage created by the interactions between the pyrimidine umbrella and phosphodianion gripper side chains (Figures 1 and 5).

Reconstruction of Wild-Type OMPDC. Table 2 shows the effects of single S154A Q215A, Y217F, and R235A mutations on $(\Delta G^{\ddagger})_{OMP}$ for decarboxylation of **OMP** determined for mutations at wild-type *Sc*OMPDC and various single, double, and triple mutants of *Sc*OMPDC. Table 2 defines a total of 32 different effects of single mutations of S154A Q215A, Y217F, and R235A on the activity of wild-type and variant *Sc*OMPDC. We focus here on the recovery in enzymatic activity observed upon substitution of wild-type amino acid side chains at the quadruple S154A/Q215A/Y217F/R235A mutant.

The substitution of single wild-type amino acids at the quadruple mutant to give triple mutants has only small effects on the stability of the decarboxylation transition state. These are shown as the bold entries in Table 2. For example, the 3.0 and 1.8 kcal/mol effects of substitution of S154 and R235 are much smaller than the 5.6 and 5.8 kcal/mol effects of these substitutions at the S154A and R235A mutant enzymes. Consequently, the sum of the effects of single S154A, Q215A, Y217F, and R235A substitutions at triple mutants of **OMPDC**, 5.6 kcal/mol (Table 2) is only 35% of the sum of the effects of these deletions at wild-type *Sc*OMPDC (16.0 kcal/mol). The small restorative effects of single substitutions at the S154A/Q215A/Y217F/R235A quadruple mutant are consistent with a large entropic cost to holding **OMPDC** in the active closed conformation. We propose that this represents the cost of fixing the positions of the pyrimidine umbrella and phosphodianion gripper loops (Figure 1) relative to the transition state.[27] In every case, a large fraction of the total binding energy of the single side chain at the triple mutants is used to pay this entropic cost, so only a small fraction remains for expression as transition state stabilization.

By contrast, the largest effects of A215Q, F217Y, and A235R substitutions on $(\Delta G^{\ddagger})_{OMP}$ (underlined text in Table 2) are observed when these side chains are incorporated into triple mutants of **OMPDC** to give the corresponding double mutant (bottom row, Table 2). For example, the A235R substitution at the Q215A/Y217F/R235A triple mutant provides for a 6.8 kcal/mol decrease in $(\Delta G^{\ddagger})_{OMP}$ compared with the smaller 5.6 kcal/mol effect of the A235R substitution at the R235A single

DOI: 10.1021/jacs.8b09609
J. Am. Chem. Soc. 2018, 140, 17580−17590

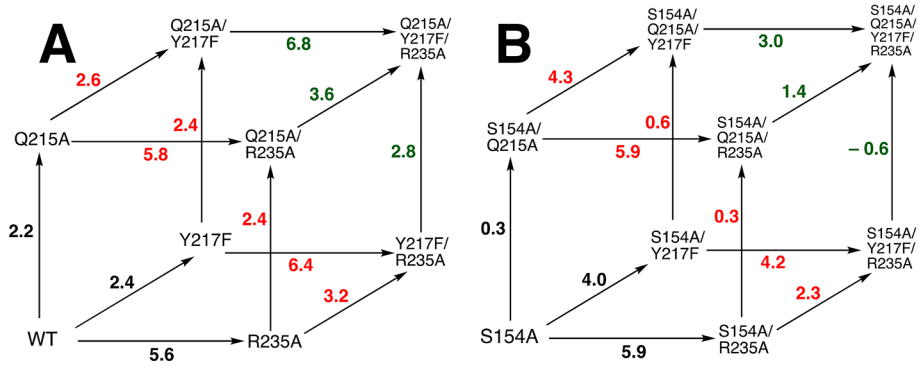

Figure 6. Triple mutant cubes that show the effects of single amino acid mutations on $(\Delta G^{\ddagger})_{OMP}$ (kcal/mol)for reactions catalyzed by wild-type *Sc*OMPDC (black values), by single mutants of *Sc*OMPDC (red values), and by double mutants of *Sc*OMPDC (green values). (A) Effect of these mutations on wild-type *Sc*OMPDC. (B) Effect of mutations on *Sc*OMPDC, previously mutated at position S154. The values of $(\Delta\Delta G_X^{\ddagger})_{OMP}$ were calculated from the ratio of the kinetic parameters k_{cat}/K_m for precursor and mutated *Sc*OMPDC-catalyzed decarboxylation of **OMP** (Table 1) and are reported in Table 2.

mutant; and, the F217Y substitution at the S154A/Q215A/Y217F triple mutant provides a 4.3 kcal/mol decrease in $(\Delta G^{\ddagger})_{OMP}$ compared with the smaller 2.4 kcal/mol effect of the F217Y substitution at the F217Y single mutant (Table 2).

The 6.8 kcal/mol effect of the A235R substitution at Q215A/Y217F/R235A *Sc*OMPDC on $(\Delta G^{\ddagger})_{OMP}$ represents the stabilizing interaction of the R235 side chain, plus an improvement in the functioning of S154 already present at the triple mutant. This cooperativity between the expression of side chain interactions reflects the roughly constant entropic cost for immobilizing the phosphodianion gripper and pyrimidine gripper loops at the active form of *Sc*OMPDC. This full price is paid by single amino acids added to the quadruple mutant, but it is split when two amino acids are added to the quadruple mutant, with the result that a larger fraction of the total binding energy of each side chain is expressed as stabilization of the decarboxylation transition state at the double mutant. An exception to this trend is the large 7.4 kcal/mol effect of the A154S substitution at the S154A/Y217F mutant shown in Figure 4B. This reflects the key role played by the clamping $-CH_2OH$ side chain of S154 in optimizing protein dianion interactions, and the large effect of the S154A mutation on the interaction of the remaining R235 side chains with the substrate dianion, as discussed above.

Smaller effects of the Q215, Y217, and R235 substitutions on $(\Delta G^{\ddagger})_{OMP}$ are observed when these side chains are inserted at double mutants of *Sc*OMPDC to give the single mutant (third row, Table 2), compared with their insertions at triple mutants to give the double mutants (bottom row, Table 2). The effects of these substitutions are then only slightly reduced when they result in wild-type *Sc*OMPDC. We propose that the interactions between any two of four side chains results in a large fractional reduction of entropy associated with loop motion and that the further entropic penalty paid upon substitution of the third side chain is small and upon substitution of the fourth side chain is negligible. Such effects are well-documented for the formation of intermolecular supramolecular complexes that are stabilized linear arrays of hydrogen bonds. The supramolecular complex stabilized by a single hydrogen bond is relatively weak, due to the large entropic penalty to the reaction between monomers to form the dimer. A larger fraction of the total stabilization from subsequent H-bonds is expressed at complexes stabilized by more than one hydrogen bond, because of the relatively small effect of each new H-bond on the total entropy of the supramolecular complex.[31]

Cubic Mutant Cycles. The data from Table 2 were used to construct the cubes shown in Figure 6. These show 24 of the 32 different effects of single substitutions from Table 2. All 32 effects may be shown on a pseudo-four-dimensional hypercube, obtained by placing the cube from Figure 6B at the center of a larger cube for Figure 6A, and drawing eight lines to connect the corners of the two cubes.[32] The last eight connections are not shown on Figure 6A,B, but several are given and discussed in our analysis of Figure 4. This hypercube is composed of eight distinct cubic cells, two of which are shown in Figure 6A,B.

Figure 6A is the previously reported cube for the effects of Q215A, Y217F, and R235A mutations on $(\Delta G^{\ddagger})_{OMP}$ for wild-type *Sc*OMPDC-catalyzed decarboxylation of **OMP**.[11] The effect of these same mutations on $(\Delta G^{\ddagger})_{OMP}$ for *Sc*OMPDC previously mutated at S154 is illustrated by Figure 6B. We concluded earlier that the effect of mutations of residue X = Q215, Y217, or R235 on $(\Delta\Delta G_X^{\ddagger})_{OMP}$ is approximately the same when the mutation is carried out at wild-type **OMPDC** or singly mutated or doubly mutated forms of **OMPDC**.[11] This shows that when S154 is present at *Sc*OMPDC, the loss of transition state stabilization from replacement of one or two side chains does not result in large changes in the stabilization by the remaining side chain(s).

By contrast, the effect of single mutations of X = Q215, Y217, or R235 on $(\Delta\Delta G_X^{\ddagger})_{OMP}$ is dependent on the context of the mutation, when the S154A mutant is the parent enzyme (Figure 6B), so that the presence of S154 is required for the regular behavior observed for Figure 6A. Figure 6B may be used to illustrate points made above in the discussion of Table 2. For example, the smallest changes in $(\Delta\Delta G_X^{\ddagger})_{OMP}$ (shown in green) are observed for single mutations of triple mutants to form the quadruple mutant; while, significantly larger changes in $(\Delta\Delta G_X^{\ddagger})_{OMP}$ (shown in red) are observed for the same mutations at double mutants to form the corresponding triple mutant.

The effects of consecutive Q215A, Y217F, and R235A mutations sum to 11.6 kcal/mol, when starting from wild-type

DOI: 10.1021/jacs.8b09609
J. Am. Chem. Soc. 2018, 140, 17580−17590

*Sc*OMPDC (Figure 6A) but to only 7.6 kcal/mol when starting from S154A mutant *Sc*OMPDC (Figure 6B). This shows that the S154A mutation results in a total (11.6−7.6) = 4.0 kcal/mol decrease in transition state stabilization from the collective interactions with the phosphodianion gripper side chain Q215, Y217, and R235. One-half (2 kcal/mol) of this decrease is due to the loss of interactions with the side chain of Q215 (Figure 4A),[15] and 2 kcal/mol results from a weakening in the interactions with Y217 and R235 (Figure 4B,C). We attribute the remaining 2 kcal/mol of the total 5.8 kcal/mol effect of the S154A mutation to the loss of the stabilizing H-bonding interaction between the S154 oxygen and the pyrimidine −NH. By comparison, the loss of this H-bonding interaction results in a 3 kcal/mol destabilization of the transition state for **OMPDC**-catalyzed decarboxylation of the phosphodianion truncated substrate **EO** (Scheme 4).[33]

SUMMARY AND CONCLUSIONS

This is the first report of an examination of the catalytic role of a network of four interacting amino acid side chains, by determining the effects of stepwise replacement of all four side chains. The four mutations result in a total (2×10^{10})-fold reduction in the activity of wild-type *Sc*OMPDC, which corresponds to the loss of 45% of the 31 kcal/mol intrinsic substrate binding energy.[3,34] The modeling of these effects of site-directed mutagenesis is a significant challenge to existing computational methods,[35] similar to that for modeling the effects of mutagenesis studies on the activity of triosephosphate isomerase.[36−43]

The relative ease of the interpretation of these experimental results reflects the choice of mobile structural elements that lie on the protein surface. A similar study is less likely to provide insight into the function of amino acid networks at the interior of protein catalysts, because of unintended structural effects of these mutations on the function of other active site catalytic side chains. The utilization of amino acid side chains, at mobile structural elements, for stabilization of enzymatic transition states is less efficient than the utilization of rigid, preorganized, side chains,[44,45] because of the entropic penalty to freezing the mobile elements at the transition state. However, flexible elements are often required to allow for the entrance and departure of ligands from active site cages.[17,46] We find that the entropic penalty to fixing the active site loops of *Sc*OMPDC (Figure 5) is a significant fraction of the interaction energy of a single side chain. This penalty is difficult to detect, and therefore easily underestimated, when it is divided between four amino acid side chains.

The mutant cubes from Figure 6A,B show that the single intraloop H-bond between the side chains of Q215 and S154 (Figure 5) has the effect of increasing the total transition state stabilization from the Q215, Y217, and R235 side chains by ca. 4 kcal/mol. These results provide a telling example of the importance of the precise placement of side chains in obtaining efficient enzymatic catalysis[47] and illustrates the magnitude of the problems that must be solved by protein engineers who are working to design proteins with enzyme-like activity.

These results are consistent with the notion that the large catalytic rate acceleration by *Sc*OMPDC is the result of many additive electrostatic interactions between the enzyme and decarboxylation transition state at a preorganized enzyme active site,[44,45,48] with two wrinkles: (1) Several amino acid side chains are not preorganized at the unliganded enzyme, but only organize after the binding of substrate, through the utilization of enzyme-dianion interactions to hold *Sc*OMPDC in a reactive caged Michaelis complex.[1,4,9,17] (2) The conversion of **OMPDC** from a flexible open form to a stiff and organized Michaelis complex results in the loss of most or all of the entropy associated with the flexible loops at the unliganded enzyme. The intrinsic substrate binding energy is utilized to pay the price for this reduction in entropy.[34]

ASSOCIATED CONTENT

Supporting Information

The Supporting Information is available free of charge on the ACS Publications website at DOI: 10.1021/jacs.8b09609.

Calculation of the concentration of **OMP** present in the Michaelis complex (E·OMP) for the initial velocity determinations; linear plot of $v/[E]$ against [FOMP] for *Ec*OMPDC-catalyzed decarboxylation of **FOMP**; plots of absorbance at 282 nm against time for decarboxylation of **FOMP** catalyzed by the S154A/Y217F, S154A/R235A, S154A/Q215A/Y217F, and the S154A/Q215A/R235A mutants of *Sc*OMPDC (PDF)

AUTHOR INFORMATION

Corresponding Author

*E-mail: jrichard@buffalo.edu.

ORCID

Archie C. Reyes: 0000-0001-9955-393X

John P. Richard: 0000-0002-0440-2387

Notes

The authors declare no competing financial interest.

ACKNOWLEDGMENTS

We acknowledge the National Institutes of Health Grants GM39754 and GM116921 (to J.P.R.) and Grant GM65155 (to J.A.G.) for generous support of this work.

REFERENCES

(1) Richard, J. P.; Amyes, T. L.; Reyes, A. C. Orotidine 5′-Monophosphate Decarboxylase: Probing the Limits of the Possible for Enzyme Catalysis. *Acc. Chem. Res.* **2018**, *51*, 960−969.

(2) Miller, B. G.; Wolfenden, R. Catalytic proficiency: the unusual case of OMP decarboxylase. *Annu. Rev. Biochem.* **2002**, *71*, 847−885.

(3) Radzicka, A.; Wolfenden, R. A proficient enzyme. *Science* **1995**, *267*, 90−93.

(4) Reyes, A. C.; Amyes, T. L.; Richard, J. Enzyme Architecture: Erection of Active Orotidine 5′-Monophosphate Decarboxylase by Substrate-Induced Conformational Changes. *J. Am. Chem. Soc.* **2017**, *139*, 16048−16051.

(5) Tsang, W.-Y.; Wood, B. M.; Wong, F. M.; Wu, W.; Gerlt, J. A.; Amyes, T. L.; Richard, J. P. Proton Transfer from C-6 of Uridine 5′-Monophosphate Catalyzed by Orotidine 5′-Monophosphate Decarboxylase: Formation and Stability of a Vinyl Carbanion Intermediate and the Effect of a 5-Fluoro Substituent. *J. Am. Chem. Soc.* **2012**, *134*, 14580−14594.

(6) Amyes, T. L.; Wood, B. M.; Chan, K.; Gerlt, J. A.; Richard, J. P. Formation and Stability of a Vinyl Carbanion at the Active Site of Orotidine 5′-Monophosphate Decarboxylase: pK_a of the C-6 Proton of Enzyme-Bound UMP. *J. Am. Chem. Soc.* **2008**, *130*, 1574−1575.

(7) Miller, B. G.; Hassell, A. M.; Wolfenden, R.; Milburn, M. V.; Short, S. A. Anatomy of a proficient enzyme: the structure of orotidine 5′-monophosphate decarboxylase in the presence and absence of a potential transition state analog. *Proc. Natl. Acad. Sci. U. S. A.* **2000**, *97*, 2011−2016.

(8) Chan, K. K.; Wood, B. M.; Fedorov, A. A.; Fedorov, E. V.; Imker, H. J.; Amyes, T. L.; Richard, J. P.; Almo, S. C.; Gerlt, J. A. Mechanism

of the Orotidine 5′-Monophosphate Decarboxylase-Catalyzed Reaction: Evidence for Substrate Destabilization. *Biochemistry* **2009**, *48*, 5518−5531.
(9) Amyes, T. L.; Malabanan, M. M.; Zhai, X.; Reyes, A. C.; Richard, J. P. Enzyme activation through the utilization of intrinsic dianion binding energy. *Protein Eng., Des. Sel.* **2017**, *30*, 159−168.
(10) Goryanova, B.; Goldman, L. M.; Ming, S.; Amyes, T. L.; Gerlt, J. A.; Richard, J. P. Rate and Equilibrium Constants for an Enzyme Conformational Change during Catalysis by Orotidine 5′-Monophosphate Decarboxylase. *Biochemistry* **2015**, *54*, 4555−4564.
(11) Goldman, L. M.; Amyes, T. L.; Goryanova, B.; Gerlt, J. A.; Richard, J. P. Enzyme Architecture: Deconstruction of the Enzyme-Activating Phosphodianion Interactions of Orotidine 5′-Monophosphate Decarboxylase. *J. Am. Chem. Soc.* **2014**, *136*, 10156−10165.
(12) Goryanova, B.; Goldman, L. M.; Amyes, T. L.; Gerlt, J. A.; Richard, J. P. Role of a Guanidinium Cation−Phosphodianion Pair in Stabilizing the Vinyl Carbanion Intermediate of Orotidine 5′-Phosphate Decarboxylase-Catalyzed Reactions. *Biochemistry* **2013**, *52*, 7500−7511.
(13) Amyes, T. L.; Ming, S. A.; Goldman, L. M.; Wood, B. M.; Desai, B. J.; Gerlt, J. A.; Richard, J. P. Orotidine 5′-monophosphate decarboxylase: Transition state stabilization from remote protein-phosphodianion interactions. *Biochemistry* **2012**, *51*, 4630−4632.
(14) Barnett, S. A.; Amyes, T. L.; McKay Wood, B.; Gerlt, J. A.; Richard, J. P. Activation of R235A Mutant Orotidine 5′-Monophosphate Decarboxylase by the Guanidinium Cation: Effective Molarity of the Cationic Side Chain of Arg-235. *Biochemistry* **2010**, *49*, 824−826.
(15) Barnett, S. A.; Amyes, T. L.; Wood, B. M.; Gerlt, J. A.; Richard, J. P. Dissecting the Total Transition State Stabilization Provided by Amino Acid Side Chains at Orotidine 5′-Monophosphate Decarboxylase: A Two-Part Substrate Approach. *Biochemistry* **2008**, *47*, 7785−7787.
(16) Reyes, A. C.; Zhai, X.; Morgan, K. T.; Reinhardt, C. J.; Amyes, T. L.; Richard, J. P. The Activating Oxydianion Binding Domain for Enzyme-Catalyzed Proton Transfer, Hydride Transfer and Decarboxylation: Specificity and Enzyme Architecture. *J. Am. Chem. Soc.* **2015**, *137*, 1372−1382.
(17) Richard, J. P.; Amyes, T. L.; Goryanova, B.; Zhai, X. Enzyme architecture: on the importance of being in a protein cage. *Curr. Opin. Chem. Biol.* **2014**, *21*, 1−10.
(18) Go, M. K.; Amyes, T. L.; Richard, J. P. Hydron Transfer Catalyzed by Triosephosphate Isomerase. Products of the Direct and Phosphite-Activated Isomerization of [1-^{13}C]-Glycolaldehyde in D_2O. *Biochemistry* **2009**, *48*, 5769−5778.
(19) Lee, J.; Goodey, N. M. Catalytic Contributions from Remote Regions of Enzyme Structure. *Chem. Rev.* **2011**, *111*, 7595−7624.
(20) First, E. A.; Fersht, A. R. Analysis of the role of the KMSKS loop in the catalytic mechanism of the tyrosyl-tRNA synthetase using multimutant cycles. *Biochemistry* **1995**, *34*, 5030−5043.
(21) Miller, B. G.; Snider, M. J.; Short, S. A.; Wolfenden, R. Contribution of Enzyme-Phosphoribosyl Contacts to Catalysis by Orotidine 5′-Phosphate Decarboxylase. *Biochemistry* **2000**, *39*, 8113−8118.
(22) Van Vleet, J. L.; Reinhardt, L. A.; Miller, B. G.; Sievers, A.; Cleland, W. W. Carbon isotope effect study on orotidine 5′-monophosphate decarboxylase: support for an anionic intermediate. *Biochemistry* **2008**, *47*, 798−803.
(23) Gross, A.; Abril, O.; Lewis, J. M.; Geresh, S.; Whitesides, G. M. Practical synthesis of 5-phospho-D-ribosyl α-1-pyrophosphate (PRPP): enzymatic routes from ribose 5-phosphate or ribose. *J. Am. Chem. Soc.* **1983**, *105*, 7428−7435.
(24) Wood, B. M.; Chan, K. K.; Amyes, T. L.; Richard, J. P.; Gerlt, J. A. Mechanism of the Orotidine 5′-Monophosphate Decarboxylase-Catalyzed Reaction: Effect of Solvent Viscosity on Kinetic Constants. *Biochemistry* **2009**, *48*, 5510−5517.
(25) Porter, D. J.T.; Short, S. A. Yeast Orotidine-5′-Phosphate Decarboxylase: Steady-State and Pre-Steady-State Analysis of the Kinetic Mechanism of Substrate Decarboxylation. *Biochemistry* **2000**, *39*, 11788−11800.
(26) Sievers, A.; Wolfenden, R. The effective molarity of the substrate phosphoryl group in the transition state for yeast OMP decarboxylase. *Bioorg. Chem.* **2005**, *33*, 45−52.
(27) Toth, K.; Amyes, T. L.; Wood, B. M.; Chan, K. K.; Gerlt, J. A.; Richard, J. P. An Examination of the Relationship between Active Site Loop Size and Thermodynamic Activation Parameters for Orotidine 5′-Monophosphate Decarboxylase from Mesophilic and Thermophilic Organisms. *Biochemistry* **2009**, *48*, 8006−8013.
(28) Moffatt, J. G. The synthesis of orotidine 5′-phosphate. *J. Am. Chem. Soc.* **1963**, *85*, 1118−23.
(29) Gasteiger, E.; Gattiker, A.; Hoogland, C.; Ivanyi, I.; Appel, R. D.; Bairoch, A. ExPASy: The proteomics server for in-depth protein knowledge and analysis. *Nucleic Acids Res.* **2003**, *31*, 3784−3788.
(30) Gasteiger, E.; Hoogland, C.; Gattiker, A.; Duvaud, A.; Wilkins, M. R.; Appel, R. D.; Bairoch, A. Protein Identification and Analysis Tools on the ExPASy Server. *Proteomics Protocols Handbook* **2005**, 571−607.
(31) Gong, B. Molecular Duplexes with Encoded Sequences and Stabilities. *Acc. Chem. Res.* **2012**, *45*, 2077−2087.
(32) Guthrie, J. P. Hydration of Carbonyl Compounds, an Analysis in Terms of Multidimensional Marcus Theory. *J. Am. Chem. Soc.* **2000**, *122*, 5529−5538.
(33) Barnett, S. A. Studies on the Mechanism of Action of Orotidine 5′-Monophosphate Decarboxylase. Ph.D. Thesis. University at Buffalo, Buffalo, NY, 2009.
(34) Jencks, W. P. Binding energy, specificity, and enzymic catalysis: the Circe effect. *Adv. Enzymol. Relat. Areas Mol. Biol.* **1975**, *43*, 219−410.
(35) Vardi-Kilshtain, A.; Doron, D.; Major, D. T. Quantum and Classical Simulations of Orotidine Monophosphate Decarboxylase: Support for a Direct Decarboxylation Mechanism. *Biochemistry* **2013**, *52*, 4382−4390.
(36) Kulkarni, Y. S.; Liao, Q.; Byléhn, F.; Amyes, T. L.; Richard, J. P.; Kamerlin, S. C. L. Role of Ligand-Driven Conformational Changes in Enzyme Catalysis: Modeling the Reactivity of the Catalytic Cage of Triosephosphate. *J. Am. Chem. Soc.* **2018**, *140*, 3854−3857.
(37) Kulkarni, Y. S.; Liao, Q.; Petrović, D.; Krüger, D. M.; Strodel, B.; Amyes, T. L.; Richard, J. P.; Kamerlin, S. C. L. Enzyme Architecture: Modeling the Operation of a Hydrophobic Clamp in Catalysis by Triosephosphate Isomerase. *J. Am. Chem. Soc.* **2017**, *139*, 10514−10525.
(38) Richard, J. P.; Amyes, T. L.; Malabanan, M. M.; Zhai, X.; Kim, K. J.; Reinhardt, C. J.; Wierenga, R. K.; Drake, E. J.; Gulick, A. M. Structure−Function Studies of Hydrophobic Residues That Clamp a Basic Glutamate Side Chain during Catalysis by Triosephosphate Isomerase. *Biochemistry* **2016**, *55*, 3036−3047.
(39) Zhai, X.; Amyes, T. L.; Richard, J. P. Role of Loop-Clamping Side Chains in Catalysis by Triosephosphate Isomerase. *J. Am. Chem. Soc.* **2015**, *137*, 15185−15197.
(40) Zhai, X.; Amyes, T. L.; Richard, J. P. Enzyme Architecture: Remarkably Similar Transition States for Triosephosphate Isomerase-Catalyzed Reactions of the Whole Substrate and the Substrate in Pieces. *J. Am. Chem. Soc.* **2014**, *136*, 4145−4148.
(41) Malabanan, M. M.; Koudelka, A. P.; Amyes, T. L.; Richard, J. P. Mechanism for Activation of Triosephosphate Isomerase by Phosphite Dianion: The Role of a Hydrophobic Clamp. *J. Am. Chem. Soc.* **2012**, *134*, 10286−10298.
(42) Malabanan, M. M.; Amyes, T. L.; Richard, J. P. Mechanism for Activation of Triosephosphate Isomerase by Phosphite Dianion: The Role of a Ligand-Driven Conformational Change. *J. Am. Chem. Soc.* **2011**, *133*, 16428−16431.
(43) Zhai, X.; Reinhardt, C. J.; Malabanan, M. M.; Amyes, T. L.; Richard, J. P. Enzyme Architecture: Amino Acid Side-Chains That Function To Optimize the Basicity of the Active Site Glutamate of Triosephosphate Isomerase. *J. Am. Chem. Soc.* **2018**, *140*, 8277−8286.

DOI: 10.1021/jacs.8b09609
J. Am. Chem. Soc. 2018, 140, 17580−17590

(44) Warshel, A.; Sharma, P. K.; Kato, M.; Parson, W. W. Modeling electrostatic effects in proteins. *Biochim. Biophys. Acta, Proteins Proteomics* **2006**, *1764*, 1647−1676.
(45) Warshel, A. Electrostatic Origin of the Catalytic Power of Enzymes and the Role of Preorganized Active Sites. *J. Biol. Chem.* **1998**, *273*, 27035−27038.
(46) Wolfenden, R. Enzyme catalysis. Conflicting requirements of substrate access and transition state affinity. *Mol. Cell. Biochem.* **1974**, *3*, 207−11.
(47) Blomberg, R.; Kries, H.; Pinkas, D. M.; Mittl, P. R.E.; Grütter, M. G.; Privett, H. K.; Mayo, S. L.; Hilvert, D. Precision is essential for efficient catalysis in an evolved Kemp eliminase. *Nature* **2013**, *503*, 418−421.
(48) Warshel, A.; Florian, J.; Strajbl, M.; Villa, J. Circe effect versus enzyme preorganization: what can be learned from the structure of the most proficient enzyme? *ChemBioChem* **2001**, *2*, 109−111.

DOI: 10.1021/jacs.8b09609
J. Am. Chem. Soc. 2018, 140, 17580−17590